Capillary climb dynamics in the limits of prevailing capillary and gravity force

B. Bijeljic,[1] B. Markicevic,[2] and H. K. Navaz[2,*]
[1]*Department of Earth Science and Engineering, Imperial College, London, SW7 2BP, United Kingdom*
[2]*Kettering University, Flint, Michigan 48504, USA*
(Received 8 February 2011; published 9 May 2011)

The dynamics of capillary climb of a wetting liquid into a porous medium that is opposed by gravity force is studied numerically. We use the capillary network model, in which an actual porous medium is represented as a network of pores and throats, each following a predefined size distribution function. The liquid potential in the pores along the liquid interface within the network is calculated as a result of capillary and gravity forces. The solution is general, and accounts for changes in the climbing height and climbing velocity. The numerical results for the capillary climb reveal that there are at least two distinct flow mechanisms. Initially, the flow is characterized by high climbing velocity, in which the capillary force is higher than the gravity force, and the flow is the viscous force dominated. For this single-phase flow, the Washburn equation can be used to predict the changes of climbing height over time. Later, for longer times and larger climbing height, the capillary and gravity forces become comparable, and one observes a slower increase in the climbing height as a function of time. Due to the two forces being comparable, the gas-liquid sharp interface transforms into flow front, where the multiphase flow develops. The numerical results from this study, expressed as the climbing height as a power law function of time, indicate that the two powers, which correspond to the two distinct mechanisms, differ significantly. The comparison of the powers with experimental data indicates good agreement. Furthermore, the power value from the Washburn solution is also analyzed, where it should be equal to $\frac{1}{2}$ for purely viscous force driven flow. This is in contrast to the power value of $\sim$0.43 that is found experimentally. We show from the numerical solution that this discrepancy is due to the momentum dissipation on the liquid interface.

DOI: 10.1103/PhysRevE.83.056310 PACS number(s): 47.56.+r

I. INTRODUCTION

Liquid imbibition in a porous medium is a pore-scale phenomenon that has received considerable attention in the field of multiphase flow owing to a large number of applications. In soil physics and plant science, unsaturated flow in which wetting fluid (water) displaces nonwetting fluid (air) is commonly encountered [1]; in petroleum engineering some oil recovery mechanisms are based on imbibition [2]; other notable applications can be found in textile engineering [3], paper coating [4], flow in fibrous filters [5], and imbibition in carbon nanotubes used in design of nanofluidic devices [6]. A commonly encountered imbibition process includes capillary force driven flow that is opposed by the gravity force, and therefore, the liquid flow occurs in a two-potential field. This two-potential flow is often referred to as capillary rise or climb. The important issue in capillary rise is the behavior of liquid in the vicinity of the region where two potentials are equal, the major question being what mechanism drives the process before the liquid flow ceases completely. Given the fact that the porous media are locally heterogeneous materials with a distribution of pore sizes, one would speculate that the flow does not stop in all points simultaneously, but rather it ceases stepwise as the liquid reaches new points whose overall potential is nonpreferable for the liquid flow to take place.

Capillary rise dynamics is driven by the interplay between capillary, gravity, and viscous forces. Pioneering efforts on determining dynamics of the advancing fluid front (height or the macroscopic position of the interface) by using analytic methods indicated the square root dependence on time [7–10]. However, in a number of experimental studies it was observed that for large times, the capillary rise height vs time dependence does not follow the parabolic behavior. Furthermore, in the experiments on the capillary rise of water through a packing of glass beads, Delker *et al.* [11] found two distinct powers, with the power at early times being larger compared to the power for longer climbing times. This two-time regime dependence of capillary rise height was also observed in the experiments in an array of packed spheres by Lago and Araujo [12]. They provide a detailed data set on the interfacial front position as well as the velocity of front propagation with time. Most importantly, at later times they observed the decay in sharpness of the saturation gradient at the interface, as opposed to the early stages of the experiment. This implies that the Washburn equation can no longer be used.

Improvements on the Washburn equation for a single capillary were suggested to include consideration of acceleration that was shown to be important only in the initial stages, as the liquid is accelerated due to the capillarity [13]. Zhmud *et al.* [14] generalized a number of equations describing capillary rise dynamics (including the Lucas-Washburn equation) by showing them to be the limiting cases of the Newton dynamics equation. However, the most interesting development is to predict the dynamics of capillary rise in the later-times regime. Lockington and Parlange [15] have solved Richard's equation which allows us to keep the dynamic saturation gradients that are ignored in the Washburn model. In their model the behavior at later times critically depends on a parameter (A) that varies with hydraulic conductivity of the medium and defines the variability in the height—this parameter has to be experimentally obtained.

*Corresponding Author: hnavaz@kettering.edu

We use a capillary network model [16,17] to represent the porous medium by preserving the statistics of pore size distribution, which is a key determinant in describing the dynamics of capillary climb. This approach is advantageous when compared to the inherent assumption in the Lucas-Washburn equation where porous medium is idealized by a bundle of single, straight line capillaries. We use a physically based description of two-phase flow in pore networks that allows us to provide the detailed analysis of the balance of capillary, gravity, and viscous forces. We explain how this balance changes with time leading to the different dynamics of capillary climb at later times, and present quantitative agreement between our model predictions and the experiments by Lago and Araujo [12] on the interfacial front position and the velocity of front propagation for bead packs and Berea sandstone.

II. MODEL SYSTEM

The schematic in Fig. 1 depicts a general problem of the wetting liquid capillary climb into a porous medium column opposed by the gravity force (g). The dynamics of how the climbing height (z) changes in time (t) may be altered by the presence of a porous medium layer placed on the bottom of the porous medium column which has thickness l and permeability K_l, and by height difference between the free liquid surface in the liquid reservoir and the zero height in the porous medium column (z_d). A wetting liquid of density ρ and viscosity μ climbs a porous medium of porosity ϕ and permeability K under the influence of the capillary pressure p_c, where p_c is defined from the liquid surface tension σ, liquid-solid contact angle θ, and characteristic radius $r_{\rm ch}$. The value of $r_{\rm ch}$ can be defined macroscopically as the square root of K/ϕ, or microscopically from the pore radius r_p. Adopting two assumptions, i.e., that the porous medium is homogeneous and the liquid-solid contact angle is not a function of the climbing velocity, the problem can be solved analytically. The solution is often referred to as the Washburn equation [10] that

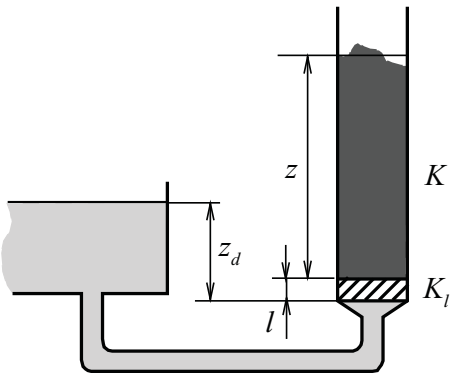

FIG. 1. Capillary climbing height (z) of wetting liquid in porous medium of permeability (K) opposed by gravity force (g) with bottom supporting layer of thickness (l) and permeability (K_l) present. The positions of zero level in porous medium ($z=0$) and reservoir liquid level (z_d) are shown.

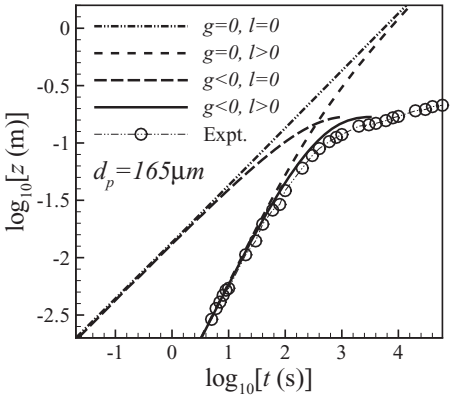

FIG. 2. Analytical solution of Eq. (1) for four combinations of both (g, l) equal to or different than zero. The maximum climbing height is defined for $g \neq 0$. The bottom layer (l, K_l) influences the slope of $\log_{10}(t)$–$\log_{10}(z)$ for small z as $z/K \approx l/K_l$, while for large z, $z/K \gg l/K_l$ and $l > 0$ approach the $l = 0$ solution.

is originally obtained for a liquid climb into a single capillary in the following form:

$$t = \frac{\mu\phi}{\rho g K}\left[\left(\frac{p_c^*}{\rho g} + \frac{K}{K_l}l\right)\ln\frac{p_c^*}{p_c^* - \rho g z} - z\right], \qquad (1)$$

where p_c^* is the capillary pressure adjusted for the hydrostatic pressures of z_d and l heights, $p_c^* = p_c + \rho g\,(z_d - l)$. The solution can be easily recast for two special cases, i.e., for the absence of the layer at the bottom of the column by setting $l = 0$, and for the capillary flow without gravity (as for the capillary flow in the horizontal porous medium bed). In this case, the analytical expression is obtained from the limiting process by setting the gravity (g) equal to zero in Eq. (1) (l'Hôpital's rule is used), where $t(l=0) = \mu\phi z^2/(2Kp_c)$ and $t(l>0) = t(l=0)[1+2Kl/(K_l z)]$.

It can be seen from Eq. (1) that in the presence of gravity, the liquid approaches a maximum climbing height ($z_{\rm max}$) for which the hydrostatic and capillary pressure are in equilibrium, and $z_{\rm max} = p_c/(\rho g) + (z_d - l)$. Equation (1) shows also that for $l = 0$ and $g = 0$, the slope of z as a function of t in logarithmic axes is equal to $\frac{1}{2}$. The $\log_{10}(t)$–$\log_{10}(z)$ plots of all four combinations (l, g), in which either l or g is equal to or different than zero are shown in Fig. 2. As expected, the initial values of climbing height are not influenced by the presence of gravity, as capillary pressure exceeds the hydrostatic pressure. For larger heights and $g<0$, both curves ($l = 0$ or $l > 0$) approach the similar $z_{\rm max}$ as $p_c/(\rho g) \gg l$, implying that $z_{\rm max}$ is not influenced by l. On the other hand, setting l (and K_l) to be greater than zero produces the $\log_{10}(t)$–$\log_{10}(z)$ curves with a slope $> \frac{1}{2}$ as the flow resistance is large in layer l, and it takes a longer time for the liquid to reach a specific height compared to the $l = 0$ case (herein, the layer l is much smaller than the overall column height and $K_l < K$). Finally, for $g = 0$, the curves corresponding to l (and K_l) equal to and greater than zero approach one another as the apparent permeability of the layer and porous medium is calculated from $(l + z)/K_{\rm app} = l/K_l + z/K$, and for sufficiently large z, $z \gg l$ and $K_{\rm app} = K$.

The porous media are heterogeneous materials with local variations of their properties, namely ϕ and K. Very often,

this fact is dealt with by defining the porous medium pore size distribution ($r_{p,i}$). Having the medium local variations, the other transport properties as capillary pressure become heterogeneous, where one needs to define a local capillary pressure distribution ($p_{c,i}$) instead of a single value of the capillary pressure defined for the average pore size. Furthermore, placing a heterogeneous porous medium into a potential field (such as gravity) produces an unstable flow as maximum climbing height becomes location specific, $z_{\max,i} = p_{c,i}/(\rho g) + (z_d - l)$. Instead of the sharp interface between the liquid and gas phase as stipulated from the Washburn equation, a liquid flow front in which liquid saturation $0 < s < 1$ is formed. The lower limit of the flow front to emerge ($z_{f,l}$) can be estimated from the maximum pore size ($r_{p,\max}$), and similarly, the upper limit of the flow front position ($z_{f,u}$) is proportional to the smallest pore ($r_{p,\min}$):

$$z_f = \frac{2\sigma\cos(\theta)}{\rho g r_{p,\mathrm{ch}}} + z_d - l, \quad \text{where } r_{p,\mathrm{ch}} = \begin{cases} r_{p,\max}, & \text{for } z_{f,l}, \\ r_{p,\min}, & \text{for } z_{f,u}. \end{cases} \tag{2}$$

The actual values of $z_{f,l}$ and $z_{f,u}$ are altered by pore connectivity within the porous medium, and $z_{f,l}$ and $z_{f,u}$ lie in between the limiting bounds calculated from Eq. (2).

III. NUMERICAL SOLUTION

Equation (2) suggests that the capillary climb dynamics are governed by two distinct flow mechanisms, the first being the single-phase climb for $z < z_{f,l}$ and the latter being the multiphase climb for $z_{f,l} < z < z_{f,u}$, where $z_{f,l}$ and $z_{f,u}$ are influenced by porous medium heterogeneity. The influence of local heterogeneities can be addressed using capillary network models [18] based on representing an actual porous medium as a network of small volumes—pores—which are connected by flow conductance elements—throats. Both pores and throats are random variables that follow some predefined distribution law. For a network consisting of ($n_x \times n_y \times n_z$) pores of volume and radius (V_p, r_p), which are connected by throats of radius and length (r_t, l_t), the network porosity (ϕ), permeability (K), and capillary pressure (p_c) for a specific liquid are calculated from

$$\phi = \frac{\sum_i V_{p,i}}{n_x n_y n_z l_{\mathrm{eq}}^3}, \quad \frac{Q}{n_x n_y l_{\mathrm{eq}}} = \frac{K}{\mu}\frac{\Delta p}{n_z}, \quad \text{and } p_{c,i} = \frac{2\sigma\cos(\theta)}{r_{p,i}}, \tag{3}$$

where Q is flow rate through the network for given pressure difference Δp, and the network equivalent length ($l_{\mathrm{eq}} = l_x/n_x = l_y/n_y = l_z/n_z$) is calculated from the geometrical dimensions of the actual porous sample ($l_x \times l_y \times l_z$). A regular cubic, three-dimensional network is depicted in Fig. 3, where the dark and light gray colors represent liquid and gas phase, respectively. Clearly, for a network to be an equivalent of the porous medium, the network and porous medium properties (ϕ, K, p_c) need to coincide.

The solution of the capillary pressure driven flows that are referred to as primary and secondary spread are explained in detail in Markicevic *et al.* [19] and Markicevic and Navaz, [17], including the problems of assemblage, boundary conditions and interface tracking. Both piston flow and snap-off flow, and their irregularities defined as gas clusters and liquid ganglia formations, are included. The solution is based on liquid phase potential at the gas-liquid interface (φ_i). Adding the gravity force, the potential (φ_i) needs to be redefined, where one can write:

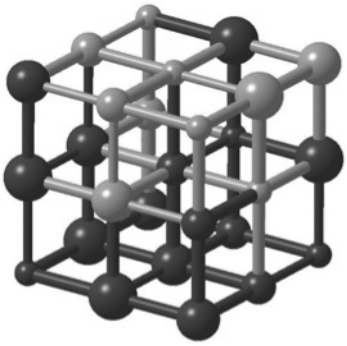

FIG. 3. A regular, three-dimensional network with each pore connected to six adjacent pores, where the radii of both pores and throats are defined from a distribution function. Two phases, gas and liquid, are represented in black and gray.

$$\varphi_i = p_{g,i} - \rho g z_i - \frac{2\sigma\cos(\theta)}{r_{p,i}}. \tag{4}$$

Based on the liquid potential of pores at the interface, the gas and liquid phase exert $p_{\mathrm{int-Gas}}$ and $p_{\mathrm{int-Liq}}$ pressure. The condition for the interface to deform is found comparing the absolute value of the pressure difference $|p_{\mathrm{int-Gas}} - p_{\mathrm{int-Liq}}|$ to the potential threshold (φ_c). Due to the presence of both capillary and gravity forces at the interface, φ_c is defined as $-\rho g z - 2\sigma\cos(\theta)/r_p$ (note that $g = -9.81\,\mathrm{m/s^2}$ in our study) and it varies along interfacial points as their climbing height and capillary pressure change. For the liquid to flow in an interfacial point, the absolute pressure between the liquid and gas phase needs to exceed the potential threshold; otherwise, the liquid remains static in that particular point.

The threshold potential varies along the interfacial pores, where depending on the pore actual potential and the threshold potential, the pore at the interface is filled or emptied. These are defined as the local flow rates at the interface and they are proportional to the difference of the capillary pressures of pores being filled and being emptied. The length scale for this flow is proportional to the multiple throat lengths, since the pairs of pores being emptied and being filled can be next to each other or bridged by some number of fully saturated pores. In parallel to the local flows at the interface, the liquid flow from the inlet to the interface takes place. This flow rate is proportional to the difference of liquid pressures at the inlet boundary and at the interface over the length scale equal to the distance of the flow front from the inlet. Depending on the ratio of the two flow rates, the formation of one of four types of pores will be favorable: (i) full ($s = 1$), (ii) empty ($s = 0$), (iii) partially filled pores ($s < 1$) which are located next to at least one full pore, and (iv) partially filled pores with all neighboring $s < 1$ pores. Hence, similarly to the general evaporation problem [20,21], four regions with distinct pore pairs saturation (s_i, s_j) can be defined: fully saturated ($s_i = s_j = 1$), highly saturated ($s_i = 1$, $s_j < 1$), low saturated ($s_i < 1$, $s_j < 1$) and nonsaturated

($s_i = s_j = 0$) regions. The numerical solution predicts the pore saturations based on the dynamic scheme, and all regions are identified directly from the numerical solution.

IV. RESULTS AND DISCUSSION

The experimental results for the capillary climb for water in four distinct porous media consisting of glass beads, and for the capillary climb in Berea sandstone, have been reported by Lago and Araujo, [12] (see also [11]). For each glass bead medium, specific sieve fractions are used, with average particle diameters (in μm), $d_p = \{165,196,231,275\}$. The glass bead porosity is measured, $\phi = 0.37$, and the permeability is estimated from the Kozeny equation and known ϕ and d_p. For Berea sandstone, $\phi = 0.22$ and $K = 1\times10^{-12}$ m^2 is reported. Both climbing height and interstitial climbing velocity, as functions of time, are measured. With respect to Fig. 1 and the physical parameters shown, all five capillary climbs are unidirectional and against the gravity force ($g < 0$). For the glass bead porous media, a thin, $l = 3$ mm, porous plate at the bottom of the column is used to keep the beads from pouring out (no such layer is used for the Berea sandstone). The layer permeability (K_l) is estimated through the time parameter, τ_p. The experimental $\log_{10}(t)$–$\log_{10}(z)$ for glass beads shows two slopes (n_1 and n_2), whereas a single slope (n) is observed for Berea sandstone. The maximum climbing height ($z_{\max}$) which is determined from the capillary and hydrostatic pressure being equal (equilibrium height, $h_{\rm eq}$ in Lago and Araujo [12]) is calculated and used in the Washburn equation. Finally, the experimental results show that the climbing height (z) reaches much larger values compared to $z_{\max}$, suggesting a change in capillary climb mechanism.

We implement the capillary network model to solve the same capillary climb dynamics for the experimental flow cases listed in the Lago and Araujo [12] study. Based on the experimental column height ($z = 0.24$ m and $z = 0.48$ m for glass beads and Berea, respectively) and computational limitations, a network consisting of $n_x \times n_y \times n_z = 20 \times 10 \times 240$ pores is generated. Hence, the network equivalent length $l_{\rm eq} = l_i/n_i$ is equal to 1 mm and 2 mm for the two porous media studied. The pore radii are set uniformly distributed, $r_{p,\min} < r_{p,i} < r_{p,\max}$, and hence, the heterogeneity parameter can be defined as $\chi = r_{p,\max}/r_{p,\min}-1$. The values of $r_{p,\min}$ and $r_{p,\max}$ for glass beads are estimated from two limiting flow front heights (z_f), as defined in Eq. (2), of the experimental $\log_{10}(t)$–$\log_{10}(z)$ curves. The lower limit $z_{f,l}$ is the height for which $\log_{10}(t)$–$\log_{10}(z)$ changes its slope. This corresponds to $r_{p,\max}$, and $r_{p,\max} = 2\sigma\cos(\theta)/(\rho g z_{f,l})$. The upper limit $z_{f,u}$ is larger than the asymptotic height that the liquid would reach if left for an infinite amount of time to climb the porous medium, and therefore, $r_{p,\min} = 2\sigma\cos(\theta)/(\rho g z_{f,u})$. This height, $z_{f,u}$, is also estimated from the experimental results and it is larger than the maximum height that the liquid front reaches. For Berea sandstone, the $\log_{10}(t)$–$\log_{10}(z)$ curve has a single slope (n) implying that the capillary pressure is significantly larger than the hydrostatic pressure for experimentally measured climbing heights. The flow is viscous force controlled. However, the $\log_{10}(t)$–$\log_{10}(z)$ curve has a slope (n) that is $< \frac{1}{2}$, and we attribute this reduced slope to the heterogeneity parameter χ. For $\chi = 0$, the slope is equal to $n = 1/2$ and the slope decreases as χ increases. This characteristic is used to find pore distribution $r_{p,\min} < r_{p,i} < r_{p,\max}$ for Berea sandstone. For the pore radius distribution defined, $r_{p,\min} < r_{p,i} < r_{p,\max}$, the network throat radii are calculated, where for two neighboring pores, i and j, the throat radius (i, j) is equal to the arithmetic average of pore radii $r_{p,i}$ and $r_{p,j}$, $r_{t,ij} = (r_{p,i}+r_{p,j})/2$. The network properties (ϕ, K, p_c) are calculated from Eq. (3) (note $V_{p,i} \propto r_{p,i}^3$) and network permeability (K) is calculated varying l_t until two permeabilities (network and porous medium) coincide [19].

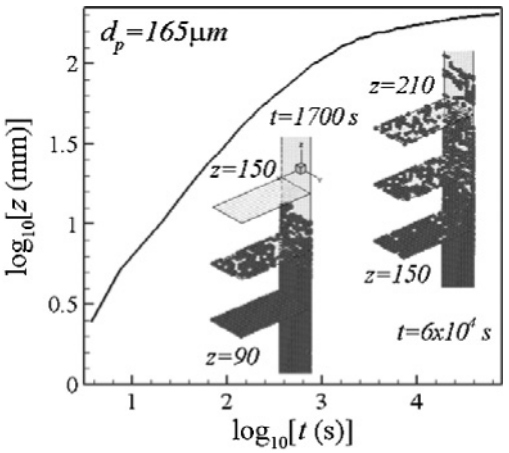

FIG. 4. Numerical solution of the climbing height as a function of time for $d_p = 165$-μm glass beads. Liquid distribution in flow front of pores that have saturation ($s > 0.95$) in the transition region and capillary (gravity) force controlled region are shown in the insets.

Having estimated the network parameters, the capillary climb is solved numerically, and the $\log_{10}(t)$–$\log_{10}(z)$ plot is shown in Fig. 4 for glass beads $d_p = 165$ μm. Two different slopes (n_1 and n_2) can be observed pointing out the transition from viscous to gravity (capillary) force dominated flow. For viscous force dominated flow, a sharp interface between gas and liquid phase exists, with a jump in liquid saturation (s) from $s = 1$ to $s = 0$. The capillary (gravity) force controlled flow produces the multiphase flow front with the liquid saturation $0 < s < 1$. The liquid distribution at the flow front is given in the two inset figures in Fig. 4 for two distinct times, $t = 1700$ s and $t = 6 \times 10^4$ s, where the liquid pore saturation is shown at the specific planes at the flow front with the dark gray pores representing $s > 0.95$. The time, $t = 1700$ s, is in the range of flow transition, and multiphase flow starts to develop with the fluid front being thin. The flow front thickness grows for the longer times, where there is a significant number of pores with $s < 0.95$ (the light gray regions). Finally, these changes in the liquid saturation for viscous and capillary (gravity) force dominated flows are also given in Fig. 5 as the axial saturation profiles $s(z)$ for three distinct times, where gas-liquid interface, flow front emergence, and full flow front developed are shown.

Equation (2) gives a measure of the pores that are filled for a particular height (z), where as the climbing height increases, the saturation gradient in the z direction decreases, and the fraction of large pores that are filled ($s > 0.95$) decreases. Therefore, the pore radius distribution function of filled pores $f_d(r_p, s > 0.95)$ within the flow front should change from being

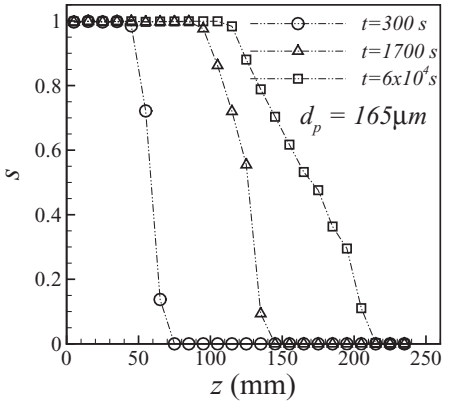

FIG. 5. Axial saturation profiles $s(z)$ for viscous force, transition, and capillary (gravity) force controlled flow for $d_p = 165$-μm glass beads.

close to the uniform for the viscous force controlled flow to a decreasing distribution function of r_p for capillary (gravity) controlled flow. Figure 6 summarizes the direct comparison between porous medium pore size distribution function $f_d(r_p)$ shown by the solid line, and corresponding $f_d(r_p,s>0.95)$, shown as a distribution histogram. Three cases are depicted in Fig. 6: (i) viscous force controlled flow for which the flow front resembles an interface (zero thickness), (ii) transition to capillary (gravity) controlled flow for which the flow front starts to develop, and (iii) capillary (gravity) force controlled flow with the flow front growing. The fraction of large pores filled decreases as the number of pores with positive threshold potential $\varphi_{c,i} = \rho g z_i - 2\sigma\cos(\theta)/r_{p,i}$ increases; here, $g = -9.81\text{m/s}^2$ and $\varphi_{c,i} < 0$ for pore i to be filled. In Fig. 6, the pore size distribution function $f_d(r_p)$ is normalized to one, where it can be seen that the fraction of large pores filled decreases. The fractions of pores with $s < 0.95$ for any r_p can also be calculated from the difference $f_d(r_p)$–$f_d(r_p,s>0.95)$ and it is always greater than zero due to the network morphology, as some small pores are shielded by larger pores and remain empty during the multiphase flow.

Furthermore, using the capillary networks with uniform size distribution, $r_{p,\min} < r_{p,i} < r_{p,\max}$, the capillary climb dynamics are solved and compared to the experimental results of Lago and Araujo [12]. In the numerical solution, both climbing height (z) and climbing velocity (v), as functions of time (t), are calculated. Since the experimental results for z and v are very close for $d_p = 196$ μm and $d_p = 231$ μm, the flow in the glass bead column with average $d_p = 231$ μm is not solved numerically for the comparison with the experiment. Thus, the three experimental cases of capillary climb in glass beads are solved numerically, where the pore sizes from the uniform distribution ($r_{p,\min}$, $r_{p,\max}$) are set equal to (27.5, 82.4), (33.1, 110) and (37.1, 180) for $d_p = 165$, 196, and 275, respectively (measured in micrometers). Furthermore, the water standard physical properties are used, and the contact angle between glass beads and water is set at $\theta = 50^\circ$ which is measured for water droplets on the solid glass surface [22]. There is an uncertainty of using this value of θ for glass bead porous medium, but it should be noted here that in the numerical calculations, the value of $\cos(\theta)/r_p$ determines the capillary

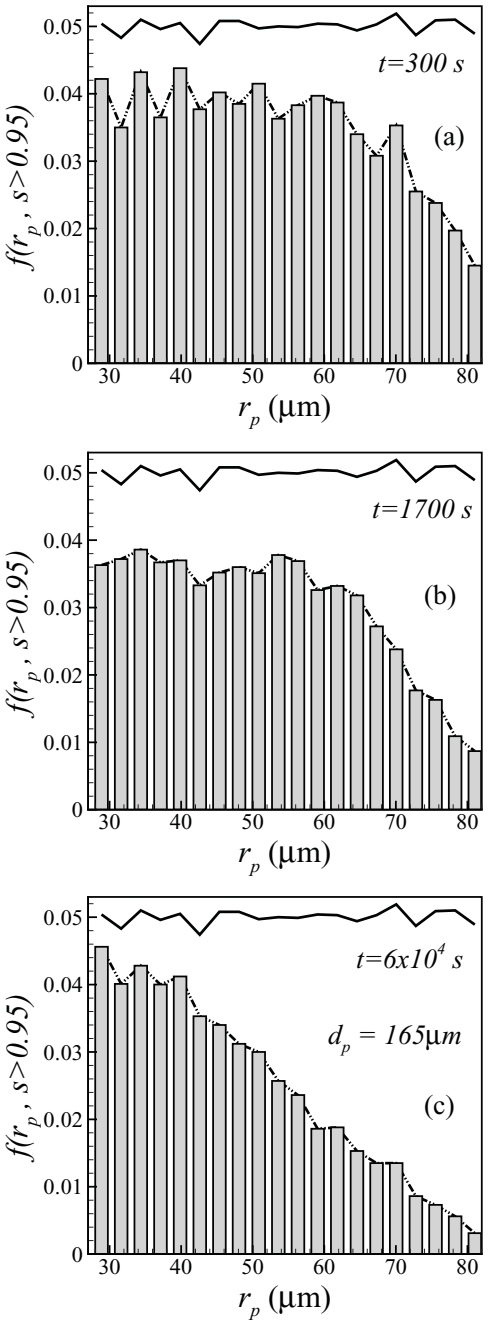

FIG. 6. Pore size distribution functions of overall sample $f_d(r_p)$ (solid lines) and distribution histogram of filled pores $f_d(r_p, s > 0.95)$, showing reduced fraction of large pores being filled during capillary (gravity) force dominated flow.

pressure. Thus, as long as $\cos(\theta)/r_p$ is predicted correctly, the numerical solution can predict the experimental results (note that the network permeability is set equal to the glass bead permeability using the throat length, l_t). For the glass bead cases, the layer of thickness $l = 3$ mm and permeability K_l is placed at the bottom of the column (see Fig. 1). The glass bead column with $d_p = 165$ μm is used to find K_l, and thereafter, the same value of K_l is set for the $d_p = 196$ μm and $d_p = 275$ μm cases. Thus, in all three numerical solutions for the distinct glass beads d_p, the value of $K_l = 4.12 \times 10^{-13}$ m^2 is defined.

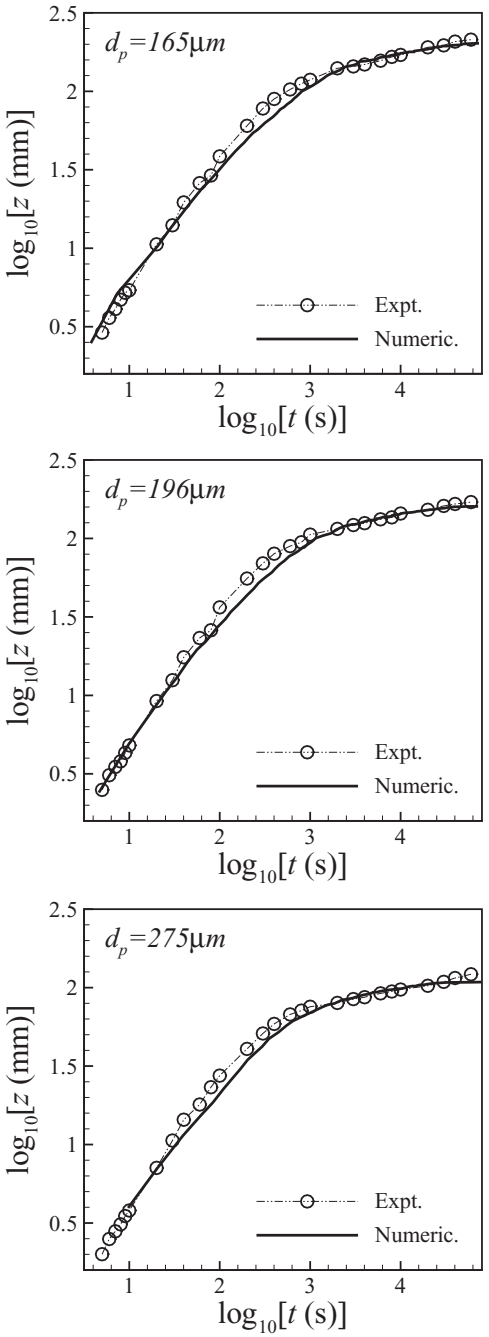

FIG. 7. Dynamics of capillary climbing flow for three distinct glass bead porous media samples: (i) $d_p = 165\ \mu$m, (ii) $d_p = 196\ \mu$m, and (iii) $d_p = 275\ \mu$m, as revealed from experimental measurements (symbols) and numerical predictions (solid lines).

The overall comparison between numerical and experimental results is shown in Figs. 7 and 8 for climbing height and velocity, respectively. In both figures, the experimental results are given with symbols that are connected by thin lines for better visibility, whereas the numerical results are shown with the thick solid lines.

It can be seen that overall there is very good agreement between the numerical predictions and the experimental results for climbing height in Fig. 7. For the viscous force controlled flow, the $z \sim t$ numerical results have slightly smaller slopes than the experimental results—this may be attributed to the (i) estimated values of the bottom layer permeability (K_l), (ii) glass bead column permeability (K), and/or (iii) pore size heterogeneity parameter (χ). On the other hand, it appears that the transition climbing height ($z_{f,l}$) for which flow mechanism changes (the slope changes from n_1 to n_2), is predicted correctly, while the flow front upper limiting height $z_{f,u}$ might be higher, as observed from the leveling off of $z \sim t$ numerical profiles. In the numerical solution we alter $z_{f,u}$ by varying $r_{p,\min}$, where a decrease of the minimum size pore radius $r_{p,\min} = 2\sigma\cos(\theta)/(\rho g z_{f,u})$ causes an increase of the capillary pressure. Hence, $r_{p,\min}$ is chosen such to produce the best overall agreement between experimental and numerical $z \sim t$ profiles and calculated slopes n_1 and n_2. All three experimental $\log_{10}(t)$–$\log_{10}(z)$ curves for distinct d_p have almost the same $n_1 = 0.80 \pm 0.01$ and $n_2 = 0.125 \pm 0.007$. Similarly, the slopes predicted numerically, $n_1 = 0.67 \pm 0.02$ and $n_2 = 0.088 \pm 0.008$, do not depend on d_p, but they are smaller compared to the experimental values. This discrepancy in slopes n_1 and n_2 may be caused by coarse network equivalent length ($l_{\mathrm{eq}} = 1$ mm), in which a broader distribution ($r_{p,\min}$, $r_{p,\max}$) needed to be prescribed in order to get sufficiently large climbing heights (z). However, this broad distribution influenced the momentum dissipation at the gas-liquid interface (or flow front) and smaller slopes are predicted from the numerical solution. Additional evidence for l_{eq} being large can be found from the numerically calculated intermittencies of climbing velocity (v) for long times, as shown in Fig. 8. These oscillations are found for small climbing velocities that are not found experimentally, again due to the large momentum dissipation. Still, there is very good agreement between experimental and numerical data. From the form of both experimental and numerical $v \sim t$ curves, one would expect three distinct flow mechanisms, namely, constant velocity and two distinct slopes of $\log_{10}(t)$–$\log_{10}(v)$ curves. However, two velocity regimes (constant and first slope) are both viscous force controlled, but with two distinct apparent permeabilities, $(l+z)/K_{\mathrm{app}} = l/K_l + z/K$. Since K_l is at least an order of magnitude smaller than K, K_{app} is not influenced by K for small z, which is not true for larger z when l/K_l and z/K become comparable.

In the experimental measurement of $z \sim t$ and $v \sim t$ profiles for Berea sandstone, the bottom supporting layer (see Fig. 1) is not used, and the $z \sim t$ solution is obtained by setting $l = 0$ into Eq. (1) (note $p_c^* = p_c + \rho g z_d$). The slope of experimental $\log_{10}(t)$–$\log_{10}(z)$ curve is $n = 0.43$, that is less than $n = 1/2$ predicted from the Washburn equation. We attribute the value of $n = 0.43$ to the medium heterogeneity, and hence momentum dissipation, where at the gas-liquid interface, local flows toward both the liquid and gas phase exist (referred to as inbound and outbound flow in Markicevic and Navaz [17]). Due to the momentum dissipation, the liquid climbing velocity is reduced. Still, the climbing velocity is high preventing the multiphase flow and fluid front to emerge. Both profiles $\log_{10}(t)$–$\log_{10}(z)$ and $\log_{10}(t)$–$\log_{10}(v)$ are shown in Fig. 9, where the experimental results are shown with the symbols and the thick solid lines represent numerically calculated profiles. Very good agreement between experimental and numerical results is found, with the slope n_n calculated from the numerical results equal to $n_n = 0.40$. The numerical

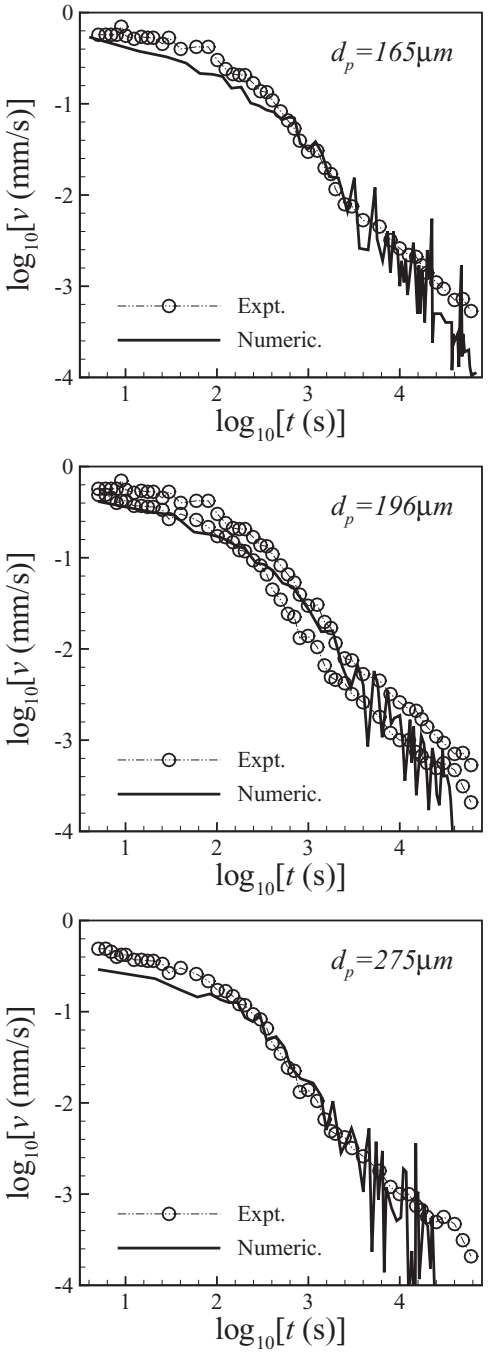

FIG. 8. Experimental and numerical climbing velocities for glass bead porous media with velocity intermittencies in the limit of slow climb. The experimental velocities for only $d_p = 165$ μm and $d_p = 275$ μm are shown.

results for $\log_{10}(t)$–$\log_{10}(z)$ are slightly curved compared to the experimental logarithmic curve, which follows a straight line.

This may be caused by our equivalent length, $l_{eq} = 2$ mm, used in the network generation, which is large for Berea sandstone due to computational limitations. Finally, additional evidence that the capillary climb for Berea sandstone is completely viscous force dominated can be seen from the

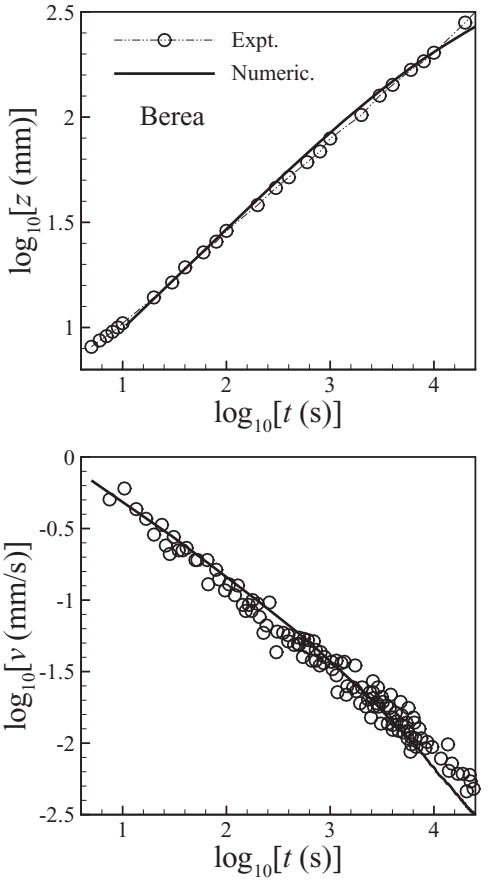

FIG. 9. Capillary climb height and velocity for the Berea sandstone with $\log_{10}(t)$–$\log_{10}(z)$ slope $< \frac{1}{2}$ ($n = 0.43$) explained by momentum dissipation at the gas-liquid interface.

velocity results, where a single slope is observed for both numerical and experimental results.

V. CONCLUSIONS

The capillary climb of a wetting liquid into a porous medium, under the influence of capillary force which is opposed by the gravity force, is formulated as a multiphase flow problem and solved numerically using the capillary network models. The time changes of the liquid climbing height and velocity reveal that there are two distinct flow mechanisms: (i) viscous and (ii) capillary (gravity) force controlled flow. The dominating force transition can be observed from the slope change in the $\log_{10}(t)$–$\log_{10}(v)$ characteristic. The viscous force controlled flow is stable, which produces the sharp interface between the liquid and gas phase. However, the unstable flow develops for capillary (gravity) force controlled flows, where the liquid and gas phase are separated with a multiphase flow front of finite thickness. The numerical formulation is compared against the experimental set of results for the capillary climb, where very good agreement is found and the experimental results have been fully explained using the numerical solution. Furthermore, even in the viscous force dominated flow, the experimental result deviations from the Washburn equation are observed. We show that the porous media heterogeneities produce the backward and forward local

flows at the interface, causing the momentum dissipation. The magnitude of the backward flow is not sufficient to transform the interface to the flow front (unstable flow), but it still can cause deviations from the Washburn equation. Thus, for the Washburn equation to be valid, it is not only sufficient that the flow is stable (existence of gas-liquid interface and not flow front), but the flow velocity needs to be high enough that the local flows at the interface can be neglected.

ACKNOWLEDGMENTS

We would like to thank and give the credit to an anonymous reviewer of our previous work for bringing this topic to our attention. We would also like to thank William Ginely at the Edgewood Chemical and Biological Center (ECBC), Sari Paikoff at Defense Threat Reduction Agency (DTRA), and Joseph Kiple of KIPLE Acquisition Science and Technology for their support throughout the Agent Fate Project.

[1] J. Bear, *Dynamics of Fluids in Porous Media* (Dover, New York, 1988).
[2] F. A. L. Dullien, *Porous Media: Fluid Transport and Pore Structure* (Academic, New York, 1992).
[3] I. Pezron, G. Bourgain, and D. Queret, J. Colloid Interface Sci. **173**, 319 (1995).
[4] J. Ghassemzadeh, M. Hashemi, L. Sartor, and M. Sahimi, AIChE J. **47**, 519 (2001).
[5] H. W. Piekaar and L. A. Clarenburg, Chem. Eng. Sci. **22**, 1399 (1967).
[6] S. Supple and N. Quirke, Phys. Rev. Lett. **90**, 214501 (2003).
[7] J. M. Bell and F. K. Cameron, J. Phys. Chem. **10**, 658 (1906).
[8] W. H. Green and G. A. Ampt, J. Agric. Sci. **4**, 1 (1911).
[9] R. Lucas, Kolloid Z. **23**, 15 (1918).
[10] E. W. Washburn, Phys. Rev. **17**, 273 (1921).
[11] T. Delker, D. B. Pengra, and P.-Z. Wong, Phys. Rev. Lett. **76**, 2902 (1996).
[12] M. Lago and M. Araujo, J. Colloid Interface Sci. **234**, 35 (2001).
[13] C. M. Reed and N. Wilson, J. Phys. D: Appl. Phys. **26**, 1378 (1993).
[14] B. V. Zhmud, F. Tiberg, and K. Hallstensson, J. Colloid Interface Sci. **228**, 263 (2000).
[15] D. A. Lockington and J. Y. Parlange, J. Colloid Interface Sci. **278**, 404 (2004).
[16] B. Markicevic and H. K. Navaz, Int. J. Numer. Methods Heat Fluid Flow **19**, 521 (2009).
[17] B. Markicevic and H. K. Navaz, Transp. Porous Media **85**, 953 (2010).
[18] I. Fatt, Trans AIME **207**, 164 (1956).
[19] B. Markicevic, T. G. D'Onofrio, and H. K. Navaz, Phys. Fluids **22**, 012103 (2010).
[20] M. Prat, Int. J. Heat Mass Transfer **50**, 1455 (2007).
[21] A. G. Yiotis, I. N. Tsimpanogiannis, A. K. Stubos, and Y. C. Yortsos, J. Colloid Interface Sci. **297**, 738 (2006).
[22] A. Skodowska and R. Matlakowska, Biotechnol. Tech. **11**, 837 (1997).